Electronic structure and magnetism of equiatomic FeN

2000 J. Phys.: Condens. Matter 12 4161

(http://iopscience.iop.org/0953-8984/12/18/302)

J. Phys.: Condens. Matter **12** (2000) 4161–4173. Printed in the UK PII: S0953-8984(00)12101-0

Electronic structure and magnetism of equiatomic FeN

Y Kong

Department of Physics and The Applied Magnetics Laboratory of the Ministry of Education, Lanzhou University, 730000 Lanzhou, China
and
Max-Planck-Institut für Festkörperforschung, Heisenbergstrasse 1, D-70569 Stuttgart, Germany

Received 24 February 2000

Abstract. In order to investigate the phase stability of equiatomic FeN compounds and the structure-dependent magnetic properties, the electronic structure and total energy of FeN with NaCl, ZnS and CsCl structures and various magnetic configurations are calculated using the first-principles TB-LMTO-ASA (tight-binding linear muffin-tin orbitals within the atomic sphere approximation) method. Among all the FeN phases considered, the antiferromagnetic (AFM) NaCl structure with $q = (0, 0, \pi)$ is found to have the lowest energy at the theoretical equilibrium volume. However, the ferromagnetic (FM) NaCl phase lies only 1 mRyd higher. The estimated equilibrium lattice constant $a^{th} = 4.36$ Å for non-magnetic (NM) ZnS-type FeN agrees quite well with the experimental value of $a^{exp} = 4.33$ Å but for the AFM NaCl phase the value $a^{th} = 4.20$ Å is 6.7% smaller than the experimentally observed 4.50 Å. For ZnS-type FeN, metastable magnetic states are found for volumes larger than the equilibrium value. On the basis of an analysis of the atom- and orbital-projected density of states and orbital-resolved crystal orbital Hamilton population, the iron–nitrogen interactions in NM ZnS, AFM NaCl and FM CsCl structures are discussed. The leading Fe–N interaction is due to the d–p iron–nitrogen hybridization, while considerable s–p and p–p hybridizations are also observed in all three phases. The iron magnetic moment μ_{Fe} in FeN is found to be highly sensitive to the nearest-neighbouring Fe–N distance. In particular, the μ_{Fe}-value shows an abrupt drop from a value of about 2 μ_B to zero with the reduction of the Fe–N distance for the ZnS and CsCl structures.

1. Introduction

For a long time, iron nitride has attracted much scientific interest, in basic research as well as in technology-oriented research. While a large number of results for iron-rich nitrides, such as γ'-Fe_4N, have appeared in the literature [1], only a few investigations on high-N-content FeN, specifically FeN [2, 3] with the proportionality 1:1 of Fe and N atoms, have been reported. Recently, two kinds of FeN structure in FeN films synthesized by the sputtering technique have been determined [4–6]. They are the sodium chloride structure with lattice constant $a = 4.5$ Å and the zinc-blende structure with lattice constant $a \approx 4.33$ Å. All the prepared FeN films were non-stoichiometric due to N vacancies and/or impurities. ^{57}Fe Mössbauer spectroscopy experiments [4, 7] have shown that at 4.2 K no magnetic hyperfine splitting is observed for ZnS-type FeN, but two kinds of Fe site in NaCl-type FeN exhibit surprisingly large hyperfine fields of 49 T and 30 T. It was suggested that the ZnS-type FeN is non-magnetic (NM) while the NaCl-type FeN shows antiferromagnetic (AFM) coupling [4, 7]. However, the magnetic measurements by Suzuki *et al* [5] indicated that at low temperature the stoichiometric ZnS-type FeN is AFM and exhibits a micromagnetic character.

0953-8984/00/184161+13$30.00

Using a full-potential linearized-augmented-plane-wave (FLAPW) method, Shimizu *et al* [8, 9] calculated the electronic, structural and magnetic properties of stoichiometric ZnS- and NaCl-type FeN and estimated the equilibrium lattice constants and bulk moduli. The results indicated that the ferromagnetic (FM) NaCl-type FeN was more stable than the NM ZnS structure. Furthermore, the calculated results [9] for the NaCl-type FeN with NM, FM, (π, π, π)- and $(0, 0, \pi)$-AFM configurations identified the FM structure as the ground state with equilibrium lattice constant $a^{th} \sim 4.0$ Å. It has further been shown that, at the experimental lattice constant 4.5 Å, the (π, π, π)-AFM state was more stable than the FM state. A similar detailed analysis was not carried out for the ZnS-type FeN and the reason for the difference in magnetism between the two structures was therefore not clear. Most recently, Eck *et al* [10] performed band-structure calculations using the tight-binding linear muffin-tin orbitals (TB-LMTO) method within the atomic sphere approximation (ASA), and investigated the structural and electronic properties of both FeN structures by analysing the density of states (DOS) and crystal orbital Hamilton population (COHP). They concluded that the zinc-blende structure should be more stable because of the weaker antibonding Fe–Fe interactions below the Fermi level. Moreover, the authors evaluated the theoretical lattice constants for non-stoichiometric FeN and found that the deficiency of N atoms decreases the equilibrium lattice constant. The magnetic properties of FeN were however hardly discussed. To achieve a better understanding of the magnetic diversity in FeN, systematic investigation of the electronic structure and magnetic properties of various FeN structures thus seems to be needed.

In this paper, the TB-LMTO-ASA method is applied to calculate band structures of FeN compounds with various structures and spin configurations. The structural, electronic and magnetic properties of the FeN are thus investigated by analysing the calculated electronic structure and total energy. In addition to the NaCl and ZnS structures, we also consider FeN in the CsCl structure.

A brief description of the computational technique will be given in the next section. In section 3, we present the calculated total energy and electronic structure, and discuss the structure and magnetic properties of FeN compounds. A short summary is given in the last section.

2. Computational details

In the present study the electronic structures of equiatomic FeN compounds are calculated self-consistently using the scalar-relativistic TB-LMTO method [12] in the atomic sphere approximation including the combined correction. A local density approximation (LDA) [13] to the density functional theory (DFT) is applied and the non-local correction is also included using the Perdew–Wang generalized-gradient approximation (GGA) [14].

The lattice structures of NaCl-, ZnS- and CsCl-type FeN compounds are illustrated in figure 1. The Fe atoms in sodium chloride and zinc-blende structures form an fcc lattice

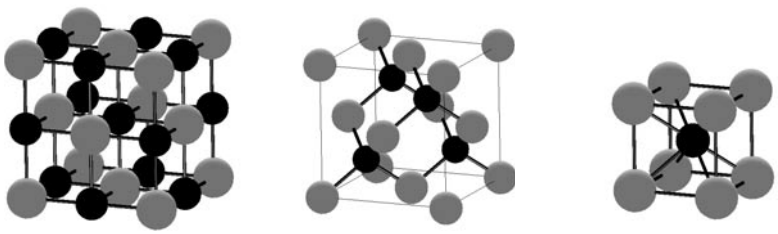

Figure 1. A schematic illustration of FeN with NaCl (left), ZnS (middle) and CsCl (right) structures.

with different coordinations of the N atoms. In the NaCl structure the N atoms are located at octahedral sites of the fcc lattice and each Fe atom has six N neighbours, while in the ZnS structure the half-filling of the N atoms in tetrahedral sites of the fcc lattice makes each Fe fourfold coordinated with N atoms. In the caesium chloride structure the N atoms fill the body-centred sites of a simple-cubic Fe lattice and one Fe is eightfold coordinated with N. The sites and filling fractions of the N atoms, the experimental magnetic structure, the nearest-neighbour (NN) Fe–Fe and Fe–N distances as well as the number of N neighbours of an Fe atom are summarized for the different structures in table 1.

Table 1. The sites and filling fractions (per cubic cell) of the N atoms in FeN compounds, lattice constants a and magnetic structures. $d_{\mathrm{Fe-Fe}}$ and $d_{\mathrm{Fe-N}}$ are the nearest-neighbour Fe–Fe and Fe–N distances at the experimental lattice constant. n is the number of N neighbours of one Fe atom. Since CsCl-type FeN does not exist, the calculated results are given.

Structure type	ZnS	NaCl	CsCl
Site	Tetrahedral	Octahedral	Body-centred
Filling fraction	4/8	4/4	1/1
Experimental magnetic structure	NM	AFM	FM
a (Å)	4.33 [4]	4.50 [4]	2.63
$d_{\mathrm{Fe-Fe}}$ (Å)	3.04	3.18	2.63
$d_{\mathrm{Fe-N}}$ (Å)	1.86	2.25	2.28
n	4	6	8

We perform NM, FM and $(0, 0, \pi)$-AFM calculations for FeN with NaCl, ZnS and CsCl structures. Besides the $(0, 0, \pi)$-AFM state, the (π, π, π)-AFM configuration and an additional AFM structure [11], which consists of double layers with FM interlayer coupling along the [001] direction, AFMD, are also considered for NaCl-type FeN to include possible magnetic coupling in FeN film. The k-space integration is performed with the tetrahedron method [15] using a $16 \times 16 \times 16$ mesh within the Brillouin zone. All partial waves with $l \leqslant 2$ are included in the basis for Fe as well as N. For ZnS- and NaCl-type FeN, special care is taken in filling the interatomic space since the structures are rather open. Therefore, it is necessary to introduce interstitial spheres. The sphere radii and the positions of the interstitial spheres are chosen in such a way that space filling is achieved without exceeding a sphere overlap of 16%. This is done using an automatic procedure developed by Krier *et al* [16]. The radii of the atomic and interstitial spheres corresponding to the theoretical equilibrium volume are listed in table 2 for the different FeN structures.

In combination with the analysis of atom- and orbital-projected density of states (DOS), the COHP technique [17] is applied to analyse the chemical bonding in ZnS-, NaCl- and CsCl-type FeN to examine the different Fe–N interactions. This technique provides information analogous to the crystal orbital overlap population (COOP) analysis [18]. While COOP curves are energy-resolved plots of the Mulliken overlap population for two atoms or orbitals, a COHP curve is an energy-resolved plot of the contribution of a given bond to the bonding energy of the system. Like for COOP curves, for all the COHP curves presented here positive values are bonding and negative ones antibonding, i.e. −COHP is plotted instead of COHP.

3. Results and discussion

3.1. Total energy and phase stability

The calculated total-energy curves for ZnS-, NaCl- and CsCl-type FeN with NM, FM and AFM spin configurations are shown in figure 2. The theoretical equilibrium lattice constants a^{th} are

Table 2. The calculated total energies, equilibrium lattice constants, DOS at E_F and Fe magnetic moments for some of the FeN structures considered. E^{th} is the total energy (given by $E + 2656.0$ in Ryd/FeN) at the theoretical equilibrium lattice constants a^{th}, $N(E_F)$ the DOS at the Fermi level in states eV^{-1}/FeN and μ_{Fe} the Fe magnetic moment at a^{th}. S_{Fe} and S_N are the radii of Fe and N atomic spheres corresponding to the theoretical equilibrium volume and S_E the radius of the interstitial sphere.

	ZnS	NaCl				CsCl	
	NM	$(0, 0, \pi)$-AFM	FM	AFMD	(π, π, π)-AFM	FM	$(0, 0, \pi)$-AFM
E^{th} (Ryd)	−0.3844	−0.3901	−0.3892	−0.3856	−0.3799	−0.3148	−0.3147
a^{th} (Å)	4.36	4.20	4.21	4.19	4.20	2.63	2.63
S_{Fe} (Å)	1.166	1.329	1.332	1.326	1.329	1.425	1.425
S_N (Å)	0.962	1.072	1.074	1.070	1.072	1.129	1.129
S_E (Å)	1.166	0.750	0.752	0.749	0.750	—	—
	0.962	—	—	—	—	—	—
μ_{Fe} (μ_B)	—	2.67	2.75	2.67	2.69	2.86	2.81
$N(E_F)$	1.40	1.90	2.42	2.39	1.03	1.57	1.98

estimated for various FeN phases and they are listed in table 2 together with total energies at a^{th}. The total energy for the NM CsCl structure is not plotted in figure 2 because the values are much higher than those for the other phases.

Firstly, we shall discuss the total-energy curves for NaCl-type FeN. Except for the NM NaCl-type FeN with higher energy, the magnetic NaCl phases with different spin configurations give similar total-energy curves. As indicated in table 2, at the equilibrium volume, E^{th} for the $(0, 0, \pi)$-AFM phase is only 1 mRyd lower than that for the FM NaCl structure and 10 mRyd below the value for the (π, π, π)-AFM structure. Although our results are in better agreement with experiment than previous results [9], a^{th} ($\sim$4.20 Å) estimated for NaCl-type FeN is still 6.7% smaller than the values observed experimentally. This discrepancy is much larger than the normal deviation due to the LDA with the GGA correction. It may therefore be, as suggested in references [9, 10], that the experimental NaCl-type FeN with $a = 4.5$ Å is not in a stable state due to unknown effects, such as the effect of the surface.

We also perform total-energy calculations for magnetic NaCl phases without the inclusion of the GGA correction to the LDA. The estimated theoretical lattice constants for magnetic NaCl phases are about 3.96–4.01 Å, and are thus smaller than those obtained with the GGA, and the FM phase is found to be stable at the theoretical equilibrium volume. The results are consistent with those given by Shimizu *et al* [9]. In the following, only the results calculated with the GGA correction are presented.

For ZnS-type FeN, a NM ground state is found with theoretical equilibrium lattice constant $a^{th} = 4.36$ Å, which agrees quite well with the experimental value [4]. The state is about 6 mRyd higher in energy than that of the $(0, 0, \pi)$-AFM NaCl structure. Self-consistent $(0, 0, \pi)$-AFM and FM solutions are found when the lattice constant is larger than 4.45 Å and 4.69 Å, respectively. Since the critical lattice constant 4.45 Å for the $(0, 0, \pi)$-AFM state is only 0.09 Å larger than a^{th} for the NM ZnS phase, one could expect the metastable AFM phase to be important for the observed micromagnetic character in ZnS-type FeN [5].

The total-energy curves calculated for FM and $(0, 0, \pi)$-AFM CsCl-type FeN are nearly identical and about 70 mRyd above those of ZnS and NaCl structures. Because of this rather higher total energy, the CsCl structure should not be considered a possible stable FeN phase.

Among all the FeN phases investigated, as mentioned above, the simple $(0, 0, \pi)$-AFM NaCl structure is found to have the lowest total energy at the theoretical equilibrium volume,

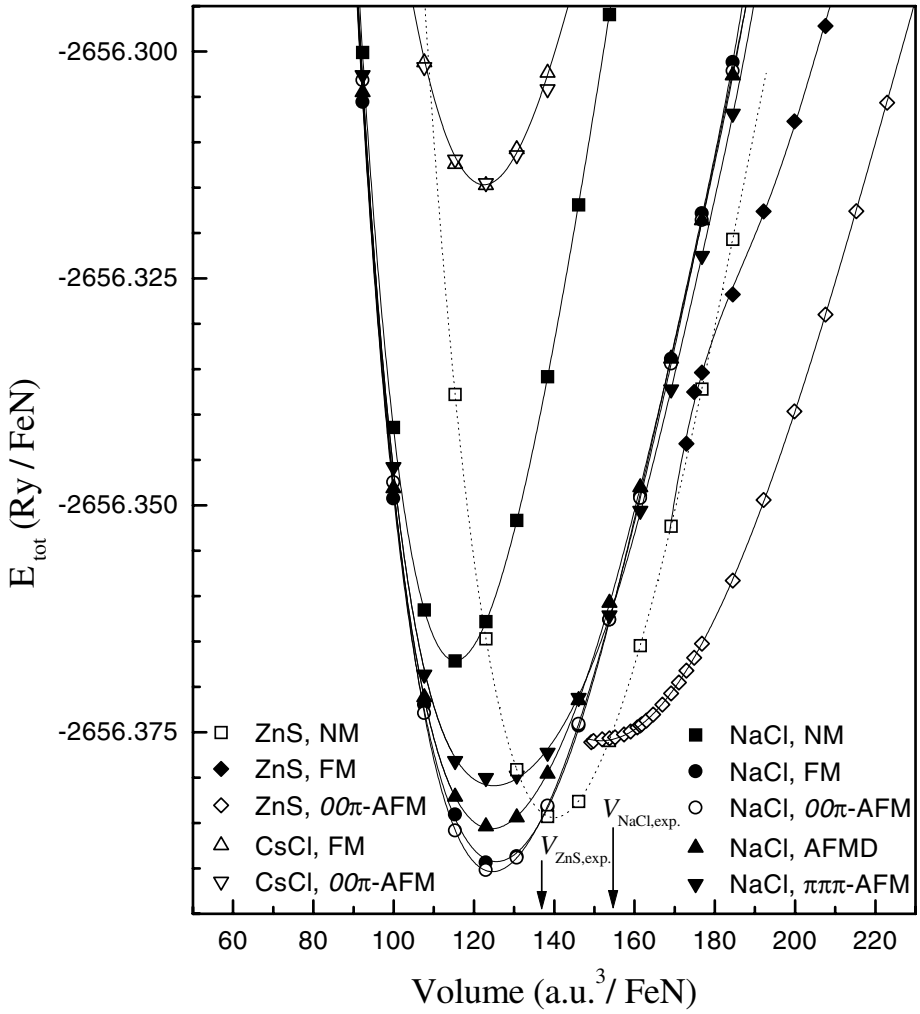

Figure 2. The calculated total energy versus volume for FeN with ZnS, NaCl and CsCl structures. Here $(0, 0, \pi)$-AFM and (π, π, π)-AFM denote phases showing antiferromagnetic coupling along [001] and [111] directions, respectively. AFMD is the AFM state which consists of double layers with FM interlayer coupling along the [001] direction. The arrows indicate the volumes corresponding to the experimental lattice constants of ZnS- and NaCl-type FeN.

while E^{th} for the FM NaCl structure is only about 1 mRyd higher. However, the energy difference is very small and may be of the order of the inaccuracies due to the ASA used in our calculations.

3.2. Electronic structure and iron–nitrogen interactions

In the following, the electronic structure and Fe–N interactions in the FeN phases will be analysed in detail using the calculated DOS and COHP for NM ZnS, $(0, 0, \pi)$-AFM NaCl and FM CsCl structures. In figure 3 we show the spin-resolved DOS for NM ZnS-, $(0, 0, \pi)$-AFM NaCl- and FM CsCl-type FeN at the theoretical equilibrium volume. The DOS at the Fermi

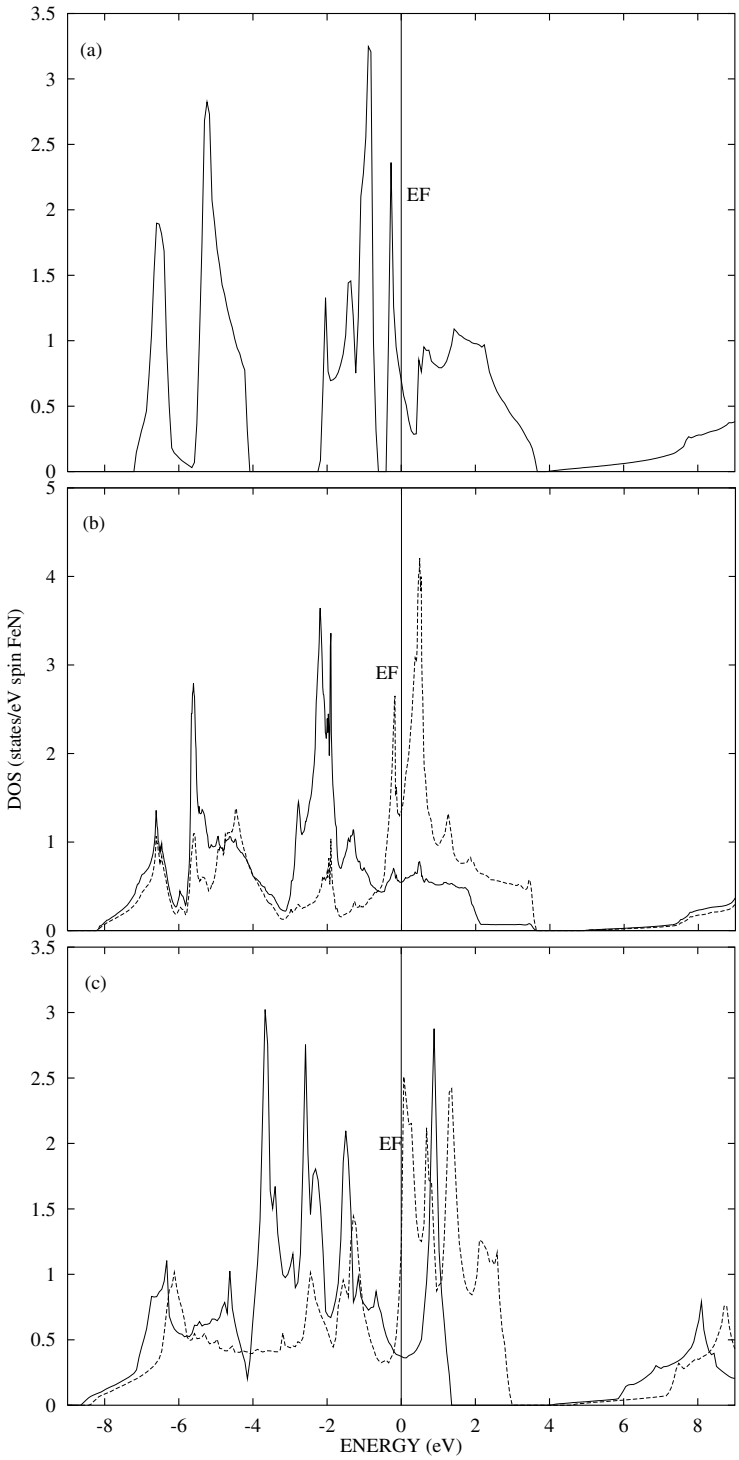

Figure 3. Spin-resolved DOS calculated for FeN with (a) non-magnetic ZnS, (b) $(0, 0, \pi)$-AFM NaCl and (c) FM CsCl structures at the theoretical equilibrium volume. Solid lines represent the majority-spin DOS and dashed lines the minority-spin DOS. The Fermi level is at zero energy.

level, $N(E_F)$, are listed in table 2.

Except for the s-like states around −15 eV, which are not shown, the DOS of the NM ZnS structure shown in figure 3(a) mainly consists of two sets of structures, which are separated by a 2 eV energy gap. The lower-energy set, centred around −6 eV, is primarily composed of N 2p bands with some admixture of Fe d character; the higher-energy set, from −2.3 to 3.6 eV, is dominated by Fe 3d states. A small gap at −0.5 eV further divides the latter into two parts, which are respectively characterized by the crystal-field-split e and t_2 sets. The Fermi level E_F is located just above the gap on the low-energy side of the t_2 set. The reason for the ZnS-type FeN phase showing no magnetic moment at equilibrium volume may be understood from the DOS at E_F. According to the Stoner model, the self-consistency condition for a ferromagnet can be simply expressed by $N(E_F)I = 1$ where $N(E_F)$ is the paramagnetic density of states at E_F and I the effective Stoner interaction parameter. For the ZnS-type FeN, it is observed that the DOS curve intersects the Fermi level with a large negative slope and gives a quite small $N(E_F)$ (0.7 states eV^{-1}/spin). Consequently, no magnetic ordering is observed for ZnS-type FeN. On the other hand, on increasing the volume, the 3d subband becomes much narrower and $N(E_F)$ larger. The Stoner criterion may therefore be satisfied and the ZnS-type FeN shows certain magnetic ordering. Indeed, our total-energy calculations for ZnS-type FeN have confirmed that metastable FM and AFM phases exist at larger volumes.

Since the band structures of the two sublattices in the AFM phase are identical, in figure 3(b) only the sublattice DOS for the $(0, 0, \pi)$-AFM NaCl structure is plotted. Unlike that of the NM ZnS phase, the DOS of $(0, 0, \pi)$-AFM NaCl-type FeN forms a continuous spectrum over the energy range between −8 and 4 eV. Due to the large dispersion of the Fe 3d subbands, the expected crystal-field splitting of 3d orbitals cannot be clearly seen. While the majority-spin DOS are nearly completely occupied, a dominant minority-spin peak is located above the Fermi level due to the exchange splitting. In figure 3(c) the peaks of the DOS for the FM CsCl structure also show a complicated structure. Compared to that of NaCl structure, the DOS of the CsCl-type FeN exhibits larger dispersion. Below E_F, the majority-spin DOS peaks of the NaCl and CsCl structures have a tendency to be split into two parts by a deep valley—at about −3 and −4 eV, respectively. The higher part is dominated by Fe 3d states while the lower one is mostly composed of N 2p states with some admixture of Fe d states.

The partial DOS (PDOS) of FeN with NM ZnS, $(0, 0, \pi)$-AFM NaCl and FM CsCl structures, projected for Fe s, p, d and N p orbitals, are plotted in figure 4. Correspondingly, figure 5 shows the orbital-projected COHP calculated for the s–p, p–p and d–p iron–nitrogen interactions. Here only the nearest-neighbour contributions are included in the COHP. Notice that of the two identical sublattices in the $(0, 0, \pi)$-AFM NaCl phase, only the PDOS for one sublattice are shown in figure 4(b) while the COHP curves for the Fe_1–N_1 (Fe_2–N_2) intra-sublattice and the Fe_1–N_2 (Fe_2–N_1) inter-sublattice interactions are presented in figures 5(b) and 5(c), respectively. Here Fe_1 (N_1) denotes the Fe (N) atom in the up-polarized sublattice and Fe_2 (N_2) the atom in the down-polarized sublattice.

Consistent with the observation of the total DOS, a 2 eV energy gap separates the PDOS of the NM ZnS phase, shown in figure 4(a), into two sets of isolated structures. As indicated by the COHP curves in figure 5(a), N p orbitals mix Fe s, p and d subbands on both sides of the gap, but the d–p hybridization dominates the iron–nitrogen interactions. The d–p Fe–N hybridization is characterized by the large bonding peaks below the gap, centred at about −5 eV, and the antibonding peaks around the Fermi level, centred at about 2.0 eV. In contrast, in both energy windows the s–p and p–p hybridizations form bonding interactions. The corresponding antibonding interactions lie far above the Fermi level.

In the $(0, 0, \pi)$-AFM NaCl structure, the PDOS projected for Fe s, p, d and N p orbitals (figure 4(b)) spread over the same energy range from −8 to 4.0 eV without an energy gap and

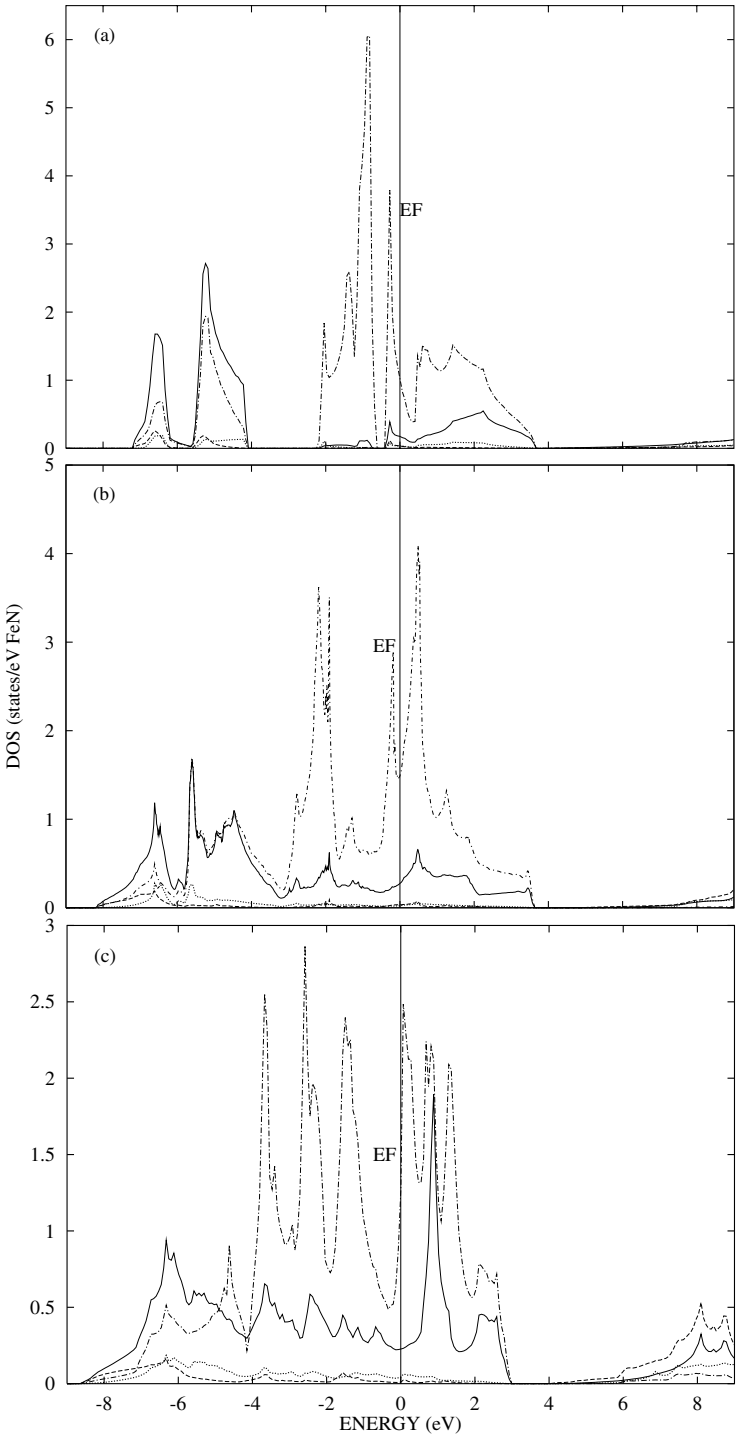

Figure 4. Orbital-projected partial DOS calculated for FeN with (a) NM ZnS, (b) $(0, 0, \pi)$-AFM NaCl and (c) FM CsCl structures at the theoretical equilibrium volume. The dashed, dotted, dash–dotted and solid lines represent the DOS projected for Fe s, p, d and N p orbitals. The Fermi level is at zero energy.

show prominent hybridizations over the entire energy range. According to the calculated COHP shown in figure 5(b) and figure 5(c), the d–p hybridization in NaCl-type FeN is characteristic of the bonding interactions below -3 eV and the antibonding states above -3 eV. Furthermore, it is found that the antibonding peaks below E_F are dominated by antibonding π^*-states and the peaks above E_F have mainly σ^*-state character. Comparing the d–p interactions in figure 5(b) and figure 5(c), a stronger antibonding π^*-peak at -2 eV is observed for inter-sublattice Fe–N hybridization. Except for the leading d–p interactions, the s–p and p–p hybridizations show considerable bonding interactions from -8 to 4 eV. In contrast to the d–p interaction, the s–p and p–p interactions for both intra- and inter-sublattice Fe–N interactions are nearly identical. Compared to the ZnS structure, the antibonding peaks of s–p and p–p hybridizations in NaCl structure are shifted towards lower energy.

Due to the larger Fe–N distance, the Fe–N interaction in the FM CsCl structure is much weaker than those in ZnS and NaCl structures. As also observed for $(0, 0, \pi)$-AFM NaCl structure, the dominant Fe–N d–p hybridization is composed of the bonding set at lower energy and the antibonding set around E_F. Below E_F there exist strong antibonding peaks. For s–p and p–p interactions the antibonding peaks are found to be much lower in energy than those in ZnS and NaCl structures.

Although the s–p and p–p hybridizations inevitably give contributions, as indicated by the COHP curves in figure 5, the dominant Fe–N interaction in all the three FeN structures is the d–p hybridization. In figure 5 we also plot the integrated COHP for d–p interactions. As indicated by the ICOHP at the Fermi level, the ZnS-type FeN exhibits the strongest d–p Fe–N hybridization among the three FeN structures because of having the shortest nearest-neighbouring Fe–N distance. In contrast, the Fe–N distance being largest in the CsCl structure causes the CsCl-type FeN to show the weakest Fe–N hybridization, although the Fe atoms in this structure have the most N neighbours.

3.3. The magnetic moment and its volume dependence

The calculated iron magnetic moments μ_{Fe} for the different FeN phases at the theoretical equilibrium volume are listed in table 2. For the four magnetic NaCl-type FeN phases, similar values of μ_{Fe} are obtained. Among these phases, the FM one produces a slightly larger value of μ_{Fe}. For both FM and AFM CsCl-type FeN, the calculated Fe magnetic moments are larger than those in NaCl-type FeN. At equilibrium volume no spin splitting for FeN with ZnS structure is obtained from spin-polarized FM and AFM calculations. Notice that the Fe–N interaction in the ZnS structure is the strongest and that in the CsCl structure the weakest; it is reasonably concluded that the magnetic properties of Fe in FeN structures are strongly correlated with the strength of the Fe–N interactions, mainly the d–p hybridization. In other words, the magnetic properties of FeN phases are closely related to the nearest-neighbouring Fe–N distance in the structure. The stronger the Fe–N hybridization is, the smaller the Fe magnetic moment becomes.

The Fe magnetic moments in magnetic NaCl-, CsCl- and ZnS-type FeN calculated at various volumes are shown in figure 6 as functions of the nearest-neighbouring Fe–N distance, $d_{\mathrm{Fe-N}}$. It is found that μ_{Fe} is highly sensitive to $d_{\mathrm{Fe-N}}$. On compressing the volume, the Fe magnetic moment in all of the magnetic FeN phases dramatically decreases with the reduction of $d_{\mathrm{Fe-N}}$. While μ_{Fe} for NaCl-type FeN decreases with $d_{\mathrm{Fe-N}}$ at nearly the same rate and gradually becomes zero as $d_{\mathrm{Fe-N}}$ becomes smaller than about 3.3 Å, μ_{Fe} exhibits a sudden drop from a value of about 2 μ_B to zero at a certain critical value of $d_{\mathrm{Fe-N}}$ for the CsCl and ZnS structures. According to the canonical band model [19], the different volume dependences of μ_{Fe} for various FeN structures should be related to the difference of the DOS around E_F.

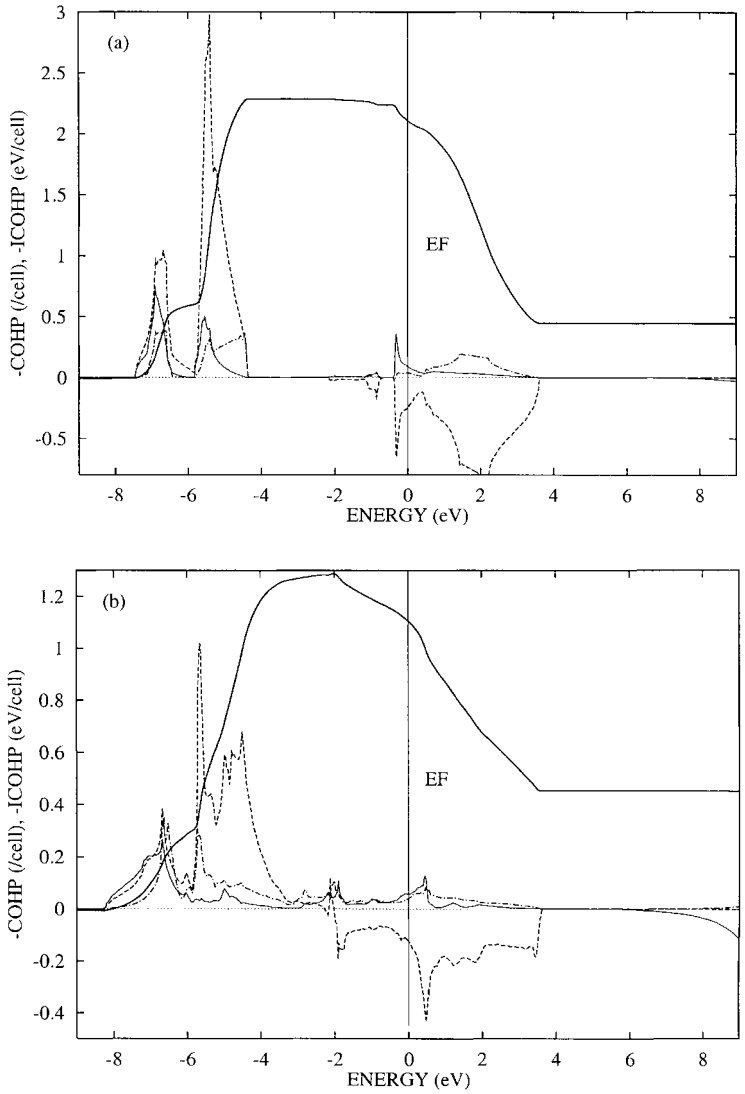

Figure 5. The COHP curves calculated for s–p, p–p and d–p interactions between Fe and N atoms in FeN with (a) NM ZnS, (b), (c) $(0, 0, \pi)$-AFM NaCl and (d) FM CsCl structures. Here (b) and (c) show the Fe–N interactions within and between the sublattices in the $(0, 0, \pi)$-AFM NaCl structure, respectively. The solid, dash–dotted and dashed lines represent s–p, p–p and d–p interactions. The integrated COHP (in eV/cell) for d–p interaction are also plotted as thick solid lines.

4. Conclusions

Starting out from the total energy and electronic structure, calculated using the TB-LMTO-ASA method, we have investigated structural, electronic and magnetic properties of FeN compounds with NaCl, ZnS and CsCl structures.

From the calculated total energy, stable $(0, 0, \pi)$-AFM NaCl-type FeN with theoretical equilibrium lattice constant $a = 4.2$ Å is identified. For FeN with ZnS structure, our results indicate the existence of metastable AFM and FM solutions with a larger cell volume besides

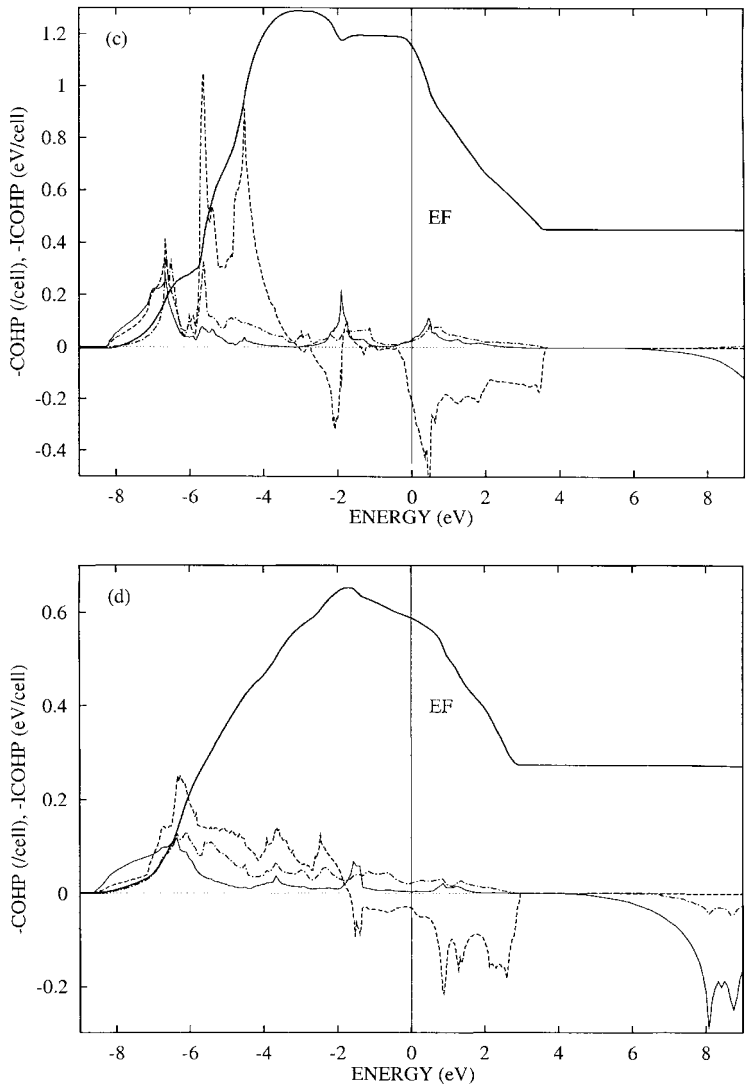

Figure 5. (Continued)

a stable NM phase. These metastable states may be important for the observed micromagnetic character in ZnS-type FeN.

On the basis of an analysis of the atom- and orbital-resolved density of states and the orbital-projected COHP, the Fe–N hybridization interactions in NM ZnS, $(0, 0, \pi)$-AFM NaCl and FM CsCl structures are discussed in detail. In all three FeN structures considered, the d–p hybridization between Fe and N atoms dominates the Fe–N interactions. On the basis of the calculated Fe magnetic moments for various FeN structures, it is suggested that the magnetic properties of FeN phases are closely related to the strength of the Fe–N d–p hybridization. Furthermore, the Fe magnetic moments in FeN phases are found to be highly sensitive to the nearest-neighbouring Fe–N distance.

Finally, it should be mentioned that the equilibrium lattice constant a^{th} estimated for NaCl-

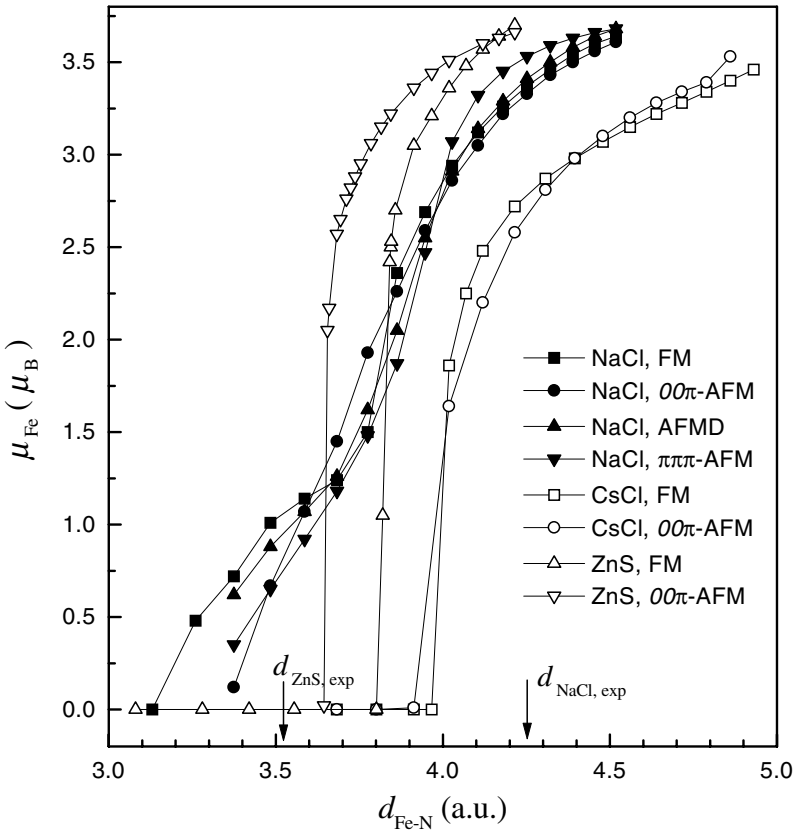

Figure 6. The calculated Fe magnetic moments in FeN with ZnS, NaCl and CsCl structures as functions of the nearest-neighbouring Fe–N distance. The arrows indicate the distances corresponding to the experimental lattice constants of NaCl- and ZnS-type FeN.

type FeN is 6.7% smaller than the values observed experimentally, though in our calculations the GGA correction to the local density approximation has been applied. It is suggested that other unknown effects may be responsible for the extraordinarily large lattice constant observed for FeN with NaCl structure. Eck *et al* [10] have estimated the equilibrium lattice constant for FeN containing defects and obtained a rather smaller value of a^{th}. To date, no theoretical investigations on FeN film have been reported. It is highly desirable for there to be calculations on the FeN structure with low-dimensional symmetry, so that the effect of surfaces may be examined.

Acknowledgments

The author would like to gratefully acknowledge Professor O K Andersen for much helpful advice and is indebted to Dr O Jepsen for a careful reading of the manuscript.

References

[1] Mohn P and Matar S F 1999 *J. Magn. Magn. Mater.* **191** 234 and the references listed therein
[2] Heiman N and Kazama N S 1981 *J. Appl. Phys.* **52** 3562

[3] Oueldennaoua A, Bauer-Grosse E, Foos M and Frants C 1985 *Scr. Metall.* **19** 1503
[4] Nakagawa H, Nasu S, Fujii H, Takahashi M and Kanamaru F 1991 *Hyperfine Interact.* **69** 455
[5] Suzuki K, Morita H, Kaneko T, Yoshida H and Fujimori H 1993 *J. Alloys Compounds* **201** 11
[6] Rissanen L, Neubauer M, Lieb K P and Schaaf P 1998 *J. Alloys Compounds* **274** 74
[7] Hinomura T and Nasu S 1998 *Hyperfine Interact.* **111** 221
[8] Shimizu H, Shirai M and Suzuki N 1997 *J. Phys. Soc. Japan* **66** 3147
[9] Shimizu H, Shirai M and Suzuki N 1998 *J. Phys. Soc. Japan* **67** 922
[10] Eck B, Dronskowski R, Takahashi M and Kikkawa S 1999 *J. Mater. Chem.* **9** 1527
[11] Herper H C, Hoffmann E and Entel P 1999 *Phys. Rev.* B **60** 3839
[12] Andersen O K and Jepsen O 1984 *Phys. Rev. Lett.* **53** 2571
Krier G, Jepsen O, Burkhardt A and Andersen O K *The Stuttgart TB-LMTO-ASA Program* Ver. 4.7
[13] Vosko S H, Wilk L and Nusair M 1980 *Can. J. Phys.* **58** 1200
[14] Perdew J P and Wang Y 1992 *Phys. Rev.* B **45** 13 244
[15] Jepsen O and Andersen O K 1971 *Solid State Commun.* **9** 1763
Jepsen O and Andersen O K 1984 *Phys. Rev.* B **29** 5965
Blöchl P, Jepsen O and Andersen O K 1994 *Phys. Rev.* B **49** 16 223
[16] Krier G, Andersen O K and Jepsen O, unpublished
[17] Dronskowski R and Blöchl P E 1993 *J. Phys. Chem.* **97** 8617
[18] Hughbanks T and Hoffmann R 1983 *J. Am. Chem. Soc.* **105** 3528
[19] Andersen O K, Madsen J, Poulsen U K, Jepsen O and Kollar J 1977 *Physica* B **86–88** 249